EPJ A
Hadrons and Nuclei

EPJ.org
your physics journal

Eur. Phys. J. A (2019) **55**: 98 DOI 10.1140/epja/i2019-12782-6

Validation of two deterministic modelings of prompt emission in fission on the basis of recent experimental data

Anabella Tudora

Società Italiana di Fisica

Springer

Eur. Phys. J. A (2019) **55**: 98
DOI 10.1140/epja/i2019-12782-6

THE EUROPEAN PHYSICAL JOURNAL A

Regular Article – Theoretical Physics

Validation of two deterministic modelings of prompt emission in fission on the basis of recent experimental data

Anabella Tudora[a]

University of Bucharest, Faculty of Physics, 405 Atomistilor Str., POB MG-11, RO-77125, Bucharest, Magurele, Romania

Received: 4 February 2019 / Revised: 9 May 2019
Published online: 26 June 2019

Communicated by P. Capel

Abstract. New experimental prompt fission neutron and fragment data for ^{235}U(n, f) measured at JRC-Geel offer the possibility of a detailed validation of the PbP and sequential emission modelings. The very good agreement of the prompt neutron multiplicity matrices $\nu(A, \mathrm{TKE})$ with these data constitutes a primary and valuable validation of the models themselves. Other data from this experiment are also well described by both model results obtained by averaging the corresponding multi-parametric matrices over an $Y(A, \mathrm{TKE})$ distribution measured at JRC-Geel. This is considered as a secondary validation (*i.e.*, of the models together with the $Y(A, \mathrm{TKE})$ distribution).

1 Introduction

The models and associated computer codes employed for nuclear data evaluation are usually validated by comparison of their results with the experimental data.

When the output quantities of the model describe well the experimental data, then the respective validation is considered as a direct (or first) validation.

In other cases the experimental data are available only for quantities, which are not the output of the respective model. To obtain these quantities which can be compared with experimental data, the output model results are used either into another model or together with other different quantities which can be either experimental data or results of other models. In this case the validation is considered as an indirect (or secondary) one.

Several computer codes with a probabilistic Monte Carlo or a deterministic treatment of prompt emission in fission, *e.g.* FIFRELIN, CGMF, FREYA, PbP, can provide —as primary results— the so-called multi-parametric matrices of different prompt emission quantities, *e.g.* prompt neutron multiplicity $\nu(A, Z, \mathrm{TKE})$, average prompt neutron energy in the center-of-mass frame $\langle\varepsilon\rangle(A, Z, \mathrm{TKE})$, prompt γ-ray energy $E_\gamma(A, Z, \mathrm{TKE})$ and multiplicity $n_\gamma(A, Z, \mathrm{TKE})$, prompt neutron spectrum in the center-of-mass frame $\Phi(\varepsilon, A, Z, \mathrm{TKE})$ and laboratory frame $N(E, A, Z, \mathrm{TKE})$ etc. Details about the prompt emission codes mentioned above can be found in the comprehensive paper [1] and references therein, as well as in subsequent publications, *e.g.* refs. [2,3] (FIFRELIN), ref. [4] (CGMF and FREYA), ref. [5] (PbP).

The comparison of such multi-parametric matrices with the existing experimental data assures a *direct (first) validation* of the prompt emission model itself. Unfortunately multi-parametric experimental data are very scarce. Only a few prompt emission quantities such as $\nu(A, \mathrm{TKE})$ and $E_\gamma(A, \mathrm{TKE})$, which were measured for only a few nuclei fissioning spontaneously or induced by thermal neutrons are available.

Experimental data concerning the single distributions of different prompt emission quantities (*e.g.* $\nu(A)$, $\nu(\mathrm{TKE})$, $\langle\varepsilon\rangle(A)$, $\langle\varepsilon\rangle(\mathrm{TKE})$, $E_\gamma(A)$, etc.) are a bit more numerous than the multi-parametric ones but they still remain insufficient. Experimental data of total average quantities, such as prompt neutron multiplicity $\langle\nu\rangle$ and prompt fission neutron spectrum in the laboratory frame $N(E)$, exist in a larger amount. The comparison with such experimental data (*i.e.*, single distributions and total average quantities) needs to average the multi-parametric matrices of different quantities generically labeled $q(A, Z, \mathrm{TKE})$ (as primary results of a prompt emission model) over a fragment distribution $Y(A, Z, \mathrm{TKE})$. The good description of such types of experimental data validates the prompt emission model together with the fragment distribution. In other words this is considered as *an indirect (or secondary) validation* of the prompt emission model.

The need of experimental data concerning prompt emission quantities in correlation with fission fragments and of fragment distribution data has encouraged the experimentalists to improve the methods and techniques for

[a] e-mail: anabellatudora@hotmail.com

the measurement of these data, an example being the team of JRC-Geel. Accurate $\nu(A, \mathrm{TKE})$ data of the first investigated case, *i.e.* ^{252}Cf(SF), were reported in 2014 by Göök *et al.* [6]. The good description of these $\nu(A, \mathrm{TKE})$ data by the results of prompt emission models, such as FIFRELIN [2], PbP [5], CGMF [4] and the deterministic modeling of sequential emission [7] was a first validation of these models.

Additional data of $\nu(A, \mathrm{TKE})$ measured by Nishio *et al.* [8] for $^{233}\mathrm{U}(\mathrm{n_{th}}, \mathrm{f})$ were also well described by the PbP and sequential emission results reported in ref. [9].

New experimental data concerning prompt neutrons in correlation with fission fragments emitted in the binary fission of ^{235}U induced by resonance neutrons were recently reported by Göök *et al.* [10]. The differences with respect to earlier data are interpreted as improved fission fragment energy resolution in the measurement performed at the GELINA facility of JRC-Geel.

These new data allow a detailed verification of the calculations for $^{235}\mathrm{U}(\mathrm{n_{th}}, \mathrm{f})$ performed with two deterministic models (PbP and the sequential emission treatment) previously reported in refs. [5,7]. In these references the model results were compared only with the experimental data available at that time for $^{235}\mathrm{U}(\mathrm{n}, \mathrm{f})$.

The present paper includes a detailed comparison of the $\nu(A, \mathrm{TKE})$ matrices provided by the PbP model and the deterministic treatment of sequential emission with the new data of Göök *et al.* [10], as well as not reported results (*e.g.*, prompt neutron spectra in the center-of-mass frame for selected fragment mass ranges and for the entire fragment mass range) which can be now compared with new experimental data.

2 Basic features focusing on the similarities and differences between the deterministic modelings of prompt emission

Because both models, PbP and the deterministic treatment of sequential emission, were already described in detail (refs. [5,7] and references therein) only a few basic features focusing on the similarities and differences between these modelings are briefly mentioned as follows.

Similarities:

a) Both models work with the same fragmentation range, which is deterministically constructed as follows. The initial fragment mass range is going from symmetric fission up to a very asymmetric split, with a step of 1 mass unit (*e.g.*, in the case of $^{235}\mathrm{U}(\mathrm{n}, \mathrm{f})$ A_H from 118 to 160 and A_L from 76 to 118). For each mass number A, three or five charge numbers Z are considered as the nearest integer values above and below the most probable charge $Zp(A)$ which is taken as the unchanged charge distribution $Z_\mathrm{UCD}(A)$ corrected with the charge polarization $\Delta Z(A)$. The charge deviation $\Delta Z(A)$ and the root-mean-square rms(A) of the isobaric charge distribution $p(Z, A)$ (taken as a Gaussian function centered on $Zp(A)$) provided by the Zp model of Wahl [11] are used. For each initial fragmentation the calculations are done at TKE values covering a large range, *e.g.* in the present case of $^{235}\mathrm{U}(\mathrm{n}, \mathrm{f})$ TKE is going from 130 to 200 MeV with a step size of 2 MeV.

b) Both models use the same partition of the total excitation energy (TXE) which is based on modeling at scission (details are given in refs. [1,12] and references therein). This TXE partition consists of the calculation of the extra-deformation energy for initial fragments at scission with respect to the full acceleration and the partition of the available excitation energy at scission between the complementary nascent fragments under the assumption of statistical equilibrium at scission and fragment level density in the Fermi gas regime.

The main difference in principle between the two modelings concerns the treatment of sequential emission.

a) In the PbP model the sequential emission is globally taken into account by a distribution of the residual temperature $P(T)$. In this case the prompt neutron spectrum in the center-of-mass frame associated to an initial fragment A, Z at a given TKE value is obtained by integrating the evaporation spectrum at a given residual temperature $\varphi(\varepsilon, T)$ over the residual temperature distribution $P(T)$, *i.e.*

$$\Phi(\varepsilon) = \int_0^{T\,\mathrm{max}} P(T)\,\varphi(\varepsilon, T)\mathrm{d}T. \qquad (1)$$

The PbP computer code allows the use of different forms for $P(T)$, either analytical expressions or numerical data (provided as input files).

b) The deterministic treatment of sequential emission described in ref. [7] is based on the recursive equations of residual temperature following the successive emission of each prompt neutron from each initial fragment A, Z of the fragmentation range at each TKE value of the TKE range, *i.e.*

$$\overline{E_r}^{(k-1)} - {S_n}^{(k-1)} - \langle\varepsilon\rangle_k = a_k\,{T_k}^2, \qquad (2)$$

in which the emission sequence is denoted by k, ${E_r}^{(k)}$ is the average energy of the k-th residual nucleus, ${S_n}^{(k)}$ is the neutron separation energy from the k-th residual nucleus, $\langle\varepsilon\rangle_k$ is the average energy in the center-of-mass frame of the k-th emitted neutron, a_k and T_k are the level density parameter and the nuclear temperature of the k-th residual nucleus, respectively. ${S_n}^{(0)}$ is the neutron separation energy from the initial fragment (before prompt neutron emission) and ${E_r}^{(0)} = E^*$ is the excitation energy of the initial fragment resulting from the TXE partition. The successive equations of residual temperature given by eq. (2) can be solved under the approximations of

non–energy-dependent level density parameters of initial and residual fragments and analytical expressions of the compound nucleus cross-sections $\sigma_c(\varepsilon)$ of the inverse process of neutron evaporation from initial and residual fragments (entering the expression of the center-of-mass energy spectrum of each emitted neutron).

The primary results of the PbP model are multi-parametric matrices of different quantities characterizing the initial fragments and the prompt emission, generically labeled $q(A, Z, \mathrm{TKE})$, *e.g.* $\nu(A, Z, \mathrm{TKE})$, $E_\gamma(A, Z, \mathrm{TKE})$, $\Phi(\varepsilon, A, Z, \mathrm{TKE})$, $\langle\varepsilon\rangle(A, Z, \mathrm{TKE})$, $N(E, A, Z, \mathrm{TKE})$ etc. The majority of experimental multi-parametric data of prompt emission are functions of A and TKE, *e.g.* $\nu(A, \mathrm{TKE})$, $E_\gamma(A, \mathrm{TKE})$ etc. For comparison with these data, the primary results $q(A, Z, \mathrm{TKE})$ are averaged over the isobaric charge distribution.

The primary results of the sequential emission modeling are multi-parametric matrices of different quantities corresponding to each emission sequence k associated to an initial fragment A, Z at a given TKE value, *i.e.* $q_k(A, Z, \mathrm{TKE})$. Multi-parametric matrices similar with the ones provided by the PbP model are obtained by averaging $q_k(A, Z, \mathrm{TKE})$ over the number of emission sequences $n(A, Z, \mathrm{TKE})$ corresponding to an initial fragment A, Z at a given TKE value, *i.e.*

$$\overline{q}(A, Z, \mathrm{TKE}) = \frac{1}{n(A, Z, \mathrm{TKE})} \sum_{k=1}^{n(A,Z,\mathrm{TKE})} q_k(A, Z, \mathrm{TKE}). \tag{3}$$

Note that the PbP model code allows the use of different prescriptions for the level density parameter of fragments, which can be energy-dependent or not. Usually the energy-dependent level density parameters provided by the super-fluid model, with different parameterizations for the asymptotic level density parameter and the damping of shell effects, are employed.

In the PbP model the compound nucleus cross-sections of the inverse process of neutron evaporation from fragments $\sigma_c(\varepsilon)$ is provided by optical model calculations with phenomenological parameterizations adequate for nuclei appearing as fission fragments (*e.g.* of Becchetti-Greenlees and Koning-Delaroche taken from RIPL3 [13]).

In the case of sequential emission treatment, the residual temperature equations (2) can be solved only for non-energy dependent level density parameter prescriptions. As it was mentioned in ref. [7] the level density parameters provided by the Egidy-Bucurescu systematic for the back-shifted Fermi gas (BSFG) model are close to the ones of the super-fluid model for the majority of initial and residual fragments (except the heavy ones with mass numbers around 130) and at a great part of excitation energies (except only the very low residual energies corresponding to the last emission sequences of several initial fragments).

In the sequential emission calculation an analytical expression of $\sigma_c(\varepsilon)$ of initial and residual fragments which depends on the s-waves neutron strength function (given by systematics) is used, details are given in ref. [7].

3 Comparison of model results with prompt neutron data recently reported

3.1 Primary model results compared with multi-parametric experimental data

The most important validation of a prompt emission model consists of the comparison of model results with experimental multi-parametric data (*e.g.* $\nu(A, \mathrm{TKE})$, $E_\gamma(A, \mathrm{TKE})$ etc.). This comparison *validates the prompt emission model itself* because the fragment distribution $Y(A, \mathrm{TKE})$ is not involved.

In the case of multi-parametric matrices of different prompt emission quantities, the best and detailed comparison is made through the 2D representations of:

- the quantity as a function of TKE for a given fragment mass A;
- the quantity as a function of A for a given TKE value.

Experimental investigations of prompt neutrons and fission fragment properties in resonance neutron induced fission on ^{235}U have been performed at the GELINA facility of JRC-Geel. The results on prompt neutron correlations with fission fragments extracted from the data by summing over the incident neutron energy range 0.26 eV–45 keV were recently reported in ref. [10]. These data offer the possibility to validate the PbP and sequential emission models themselves (*i.e.*, without the involvement of fragment distributions $Y(A, \mathrm{TKE})$).

The experimental matrix of prompt neutron multiplicity $\nu(A, \mathrm{TKE})$ measured by Göök *et al.* in the representation of prompt neutron multiplicity as a function of TKE for a given fragment mass is plotted in figs. 1 and 2 with open black squares for A_L, full gray circles for A_H and full black diamonds for the fragment mass pair. These data are compared with the PbP model result in fig. 1 (in which the parts (a)–(c) include almost all mass fragmentations) and with the sequential emission result in fig. 2 (exemplified for 9 fragmentations covering the entire mass range). In both figures the model results are plotted with continuous lines colored in green (light fragments), blue (heavy fragments) and red (fragment pairs).

The experimental matrix $\nu(A, \mathrm{TKE})$ in the representation of prompt neutron multiplicity as a function of mass and prompt neutron multiplicity of the fragment pair as a function of A_H, both for a given value of TKE (mentioned in the legend of each frame) is plotted with full black squares in figs. 3 and 4. These data are compared with the PbP result (red circles) in fig. 3 and with the result of the sequential emission treatment (blue stars) in fig. 4.

The excellent description of the experimental data by the PbP result is easily seen in figs. 1 and 3.

In figs. 1–4 it can be also observed that for fragmentations near symmetry (A_H less than 133 and A_L great than 103) the experimental data at lower TKE values are scattered, with large error bars and they deviate from the linear trend (see fig. 1), this behaviour being due to the low yield and the contamination of background events [14].

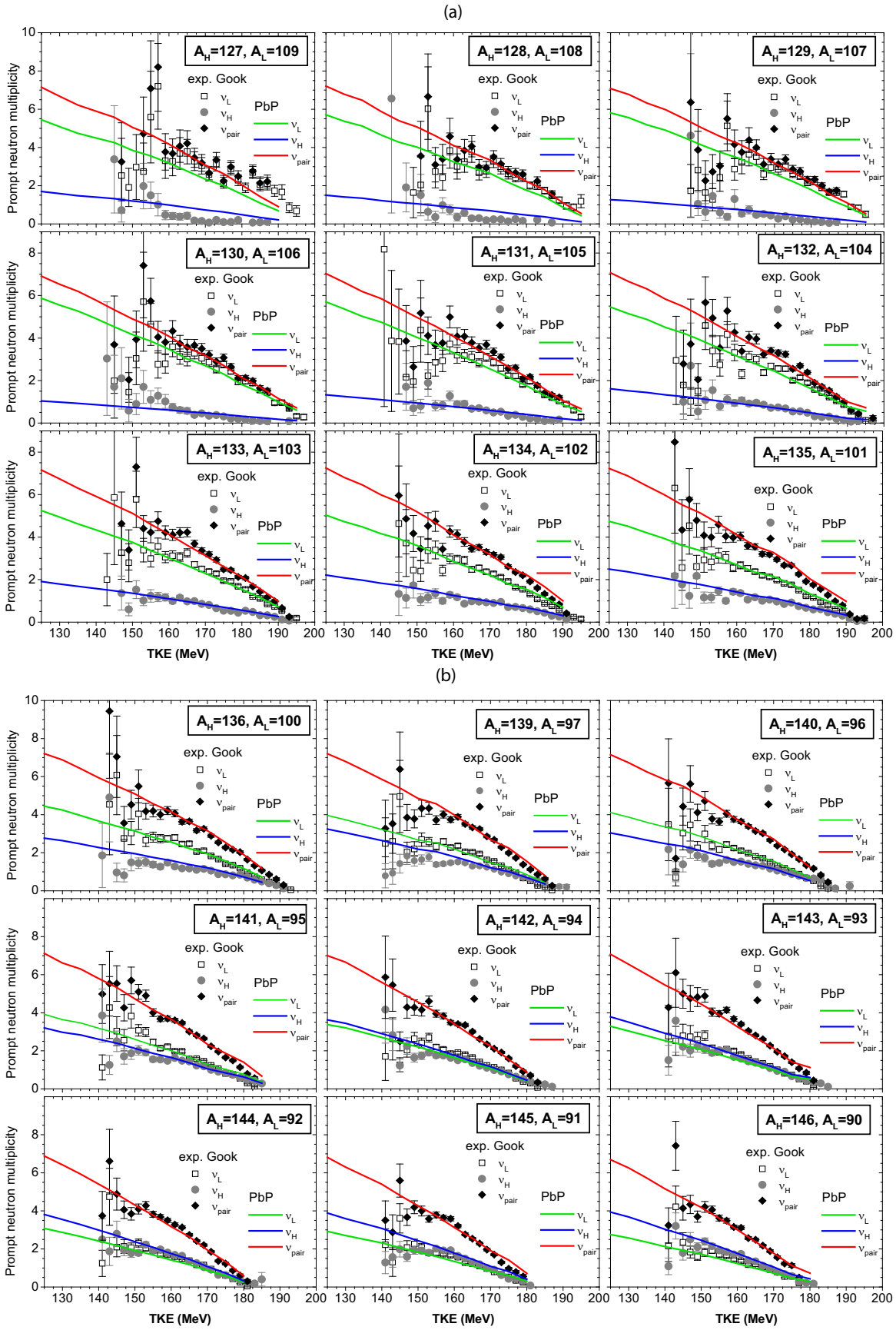

Fig. 1. (a)–(c): Comparison of $\nu(A, \mathrm{TKE})$ results of PbP (lines) for $^{235}\mathrm{U}(\mathrm{n_{th}}, \mathrm{f})$ with the data of Göök *et al.* (symbols) in the representation of prompt neutron multiplicity as a function of TKE for the masses indicated in each frame.

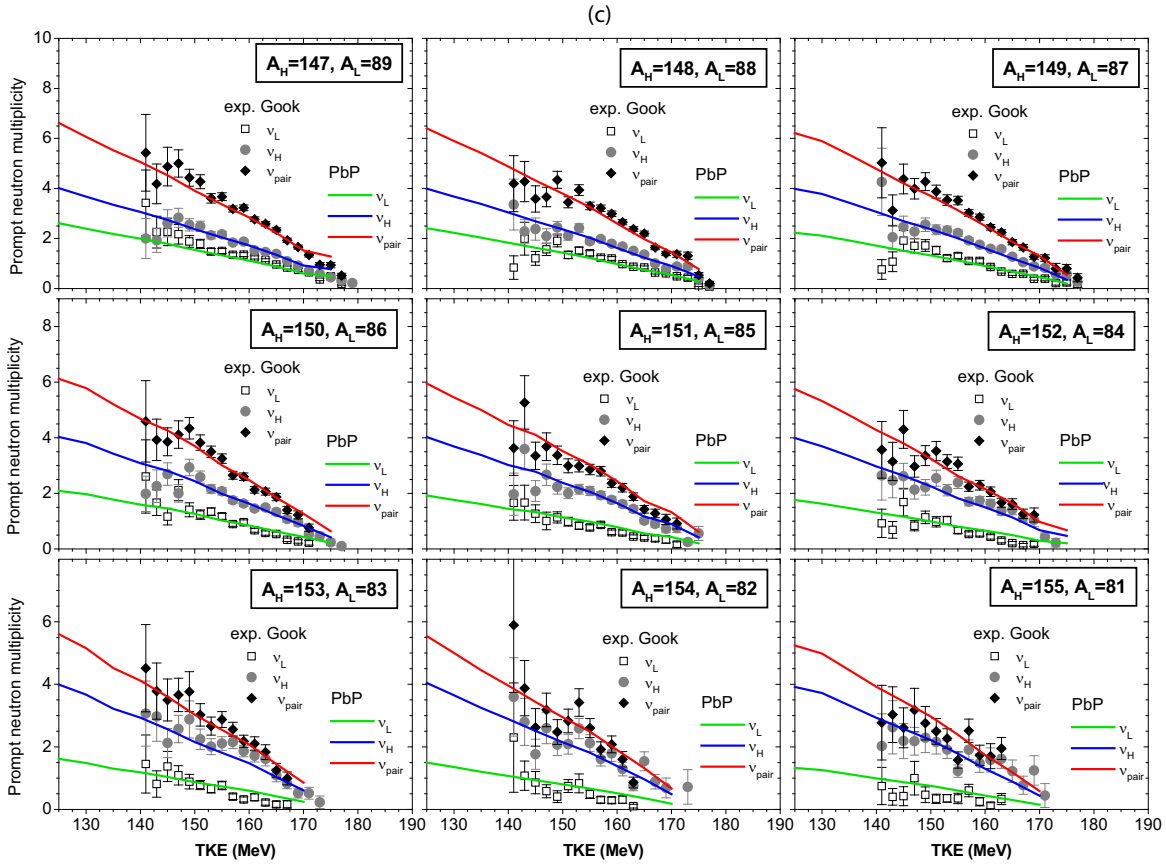

Fig. 1. Continued.

In the case of sequential emission results the agreement with the experimental data of Göök *et al.* is also very good but not as remarkable as in the case of PbP results plotted in fig. 1. An explanation of the staggering exhibited by the $\nu(A, \mathrm{TKE})$ results of fig. 2 is due to the limited number of initial fragments taken into account in the treatment of sequential emission, *i.e.* 3 charge numbers Z at each A. This fact is visible especially for initial fragmentations with A_{H} around 130 for which the heavy fragments (often magic or doubly magic, *i.e.* $Z = 50$, $N = 82$) frequently cannot emit prompt neutrons, leading to very low values of the prompt neutron multiplicity corresponding to the heavy fragment mass number. The same situation is also happening for many fragmentations at high TKE values, *i.e.* the excitation energy of fully accelerated complementary fragments being often too low, the prompt neutron emission becoming impossible. In the case of PbP, even if the fragmentation range is the same (*i.e.* also 3 charge numbers Z per A), this situation is avoided by the global treatment of the sequential emission using the residual temperature distribution $P(T)$ which covers the entire process of successive neutron emission corresponding to each initial fragment. Sequential emission calculations performed with an initial fragmentation range in which 5 charge numbers Z are taken at each A lead to a less pronounced staggering in the $\nu(A, \mathrm{TKE})$ results, the agreement with the experimental data is improved but it is not as the same remarkable level as in the case of PbP results. This is due to the sequential emission modeling itself, *i.e.* an event-by-event treatment in which the successive transcendent equations of residual temperatures were solved under some assumptions [7], *e.g.* the approximation of non-energy dependent level density parameters of initial and residual fragments, compared to the global treatment of PbP based on a $P(T)$ distribution and the use of energy-dependent level density parameters of the super-fluid model.

The $\nu(A, \mathrm{TKE})$ results compared in figs. 1–4 with the recent experimental data of Göök *et al.* are the ones of the PbP and sequential emission calculations performed in 2016 and 2017 for which only average prompt emission results (*i.e.* as single distributions or total average quantities) in comparison with the experimental data existing at that time were reported in refs. [5] and [7].

In other words, up to now the PbP and sequential emission calculations for $^{235}\mathrm{U}(\mathrm{n_{th}}, \mathrm{f})$ were only indirectly validated, *i.e.* together with the experimental fragment distribution used at that time and only partially by comparison with older experimental data available at that time for a limited number of quantities.

Consequently the prompt neutron multiplicity matrices, as primary results of the previous PbP and sequential emission calculations, are confirmed by the subsequent experimental data of Göök *et al.* [10]. This fact constitutes a valuable validation of these deterministic modelings of prompt emission.

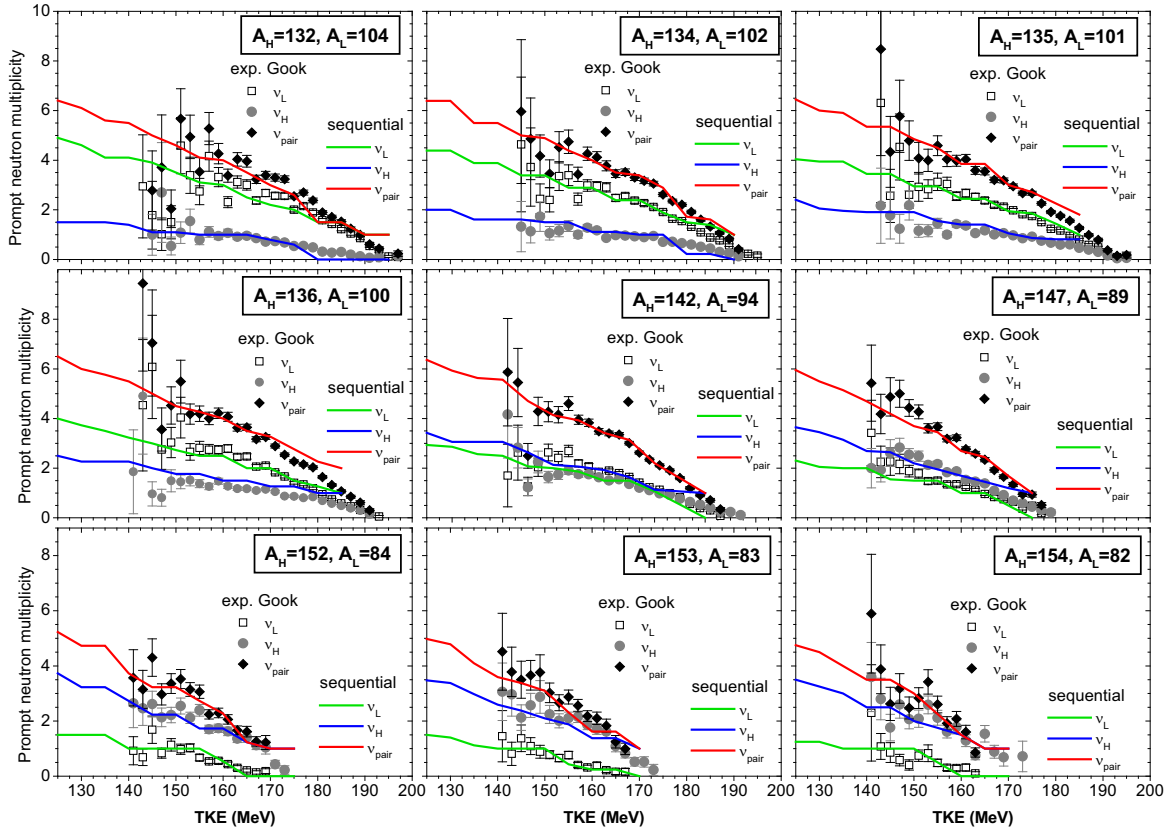

Fig. 2. Comparison of $\nu(A, \mathrm{TKE})$ results of the sequential emission treatment (lines) for $^{235}\mathrm{U}(\mathrm{n_{th}}, \mathrm{f})$ with the data of Göök *et al.* (symbols) in the representation of prompt neutron multiplicity as a function of TKE for the masses indicated in each frame.

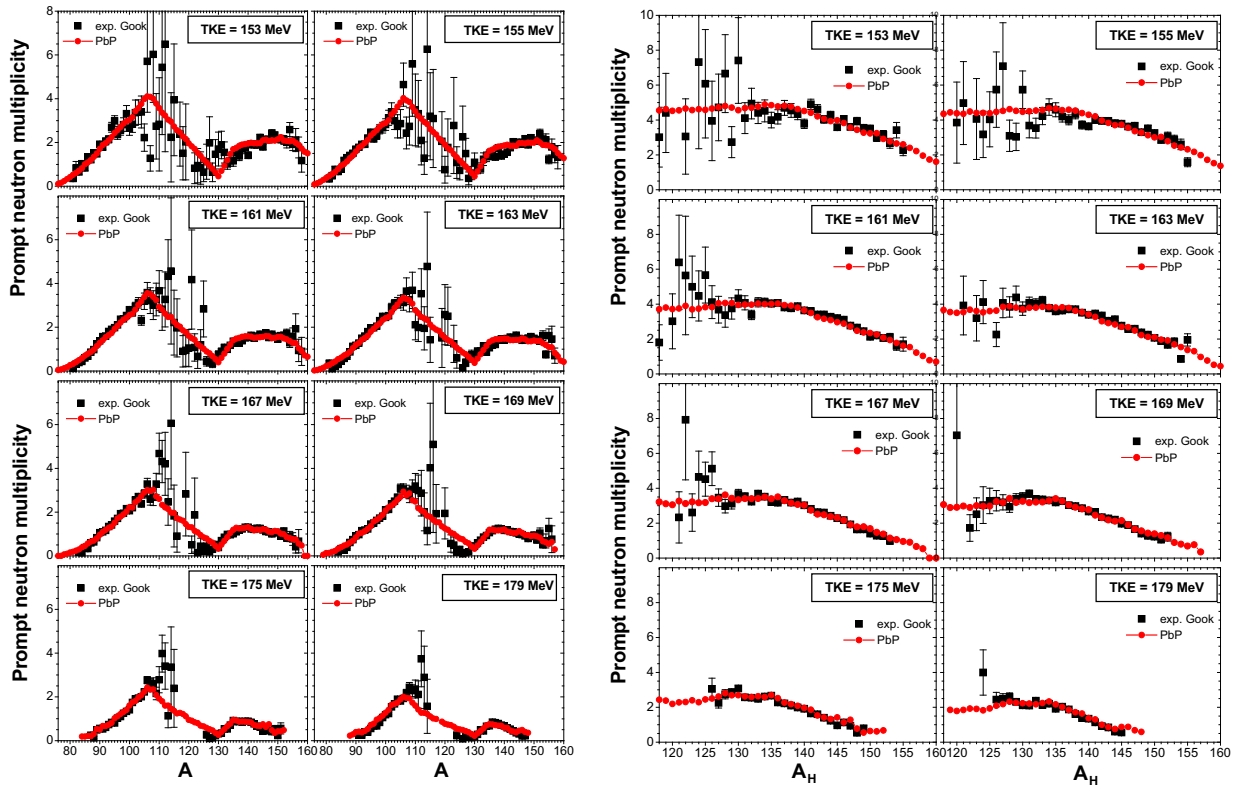

Fig. 3. Comparison of the $\nu(A, \mathrm{TKE})$ matrix of PbP (red circles) for $^{235}\mathrm{U}(\mathrm{n_{th}}, \mathrm{f})$ with the data of Göök *et al.* (black squares) in the representation of the prompt neutron multiplicity as a function of A (left part) and the prompt neutron multiplicity of a fragment pair as a function of A_{H} (right part) at the TKE values indicated in each frame. The lines connecting the points plotted with red circles are only to guide the eye.

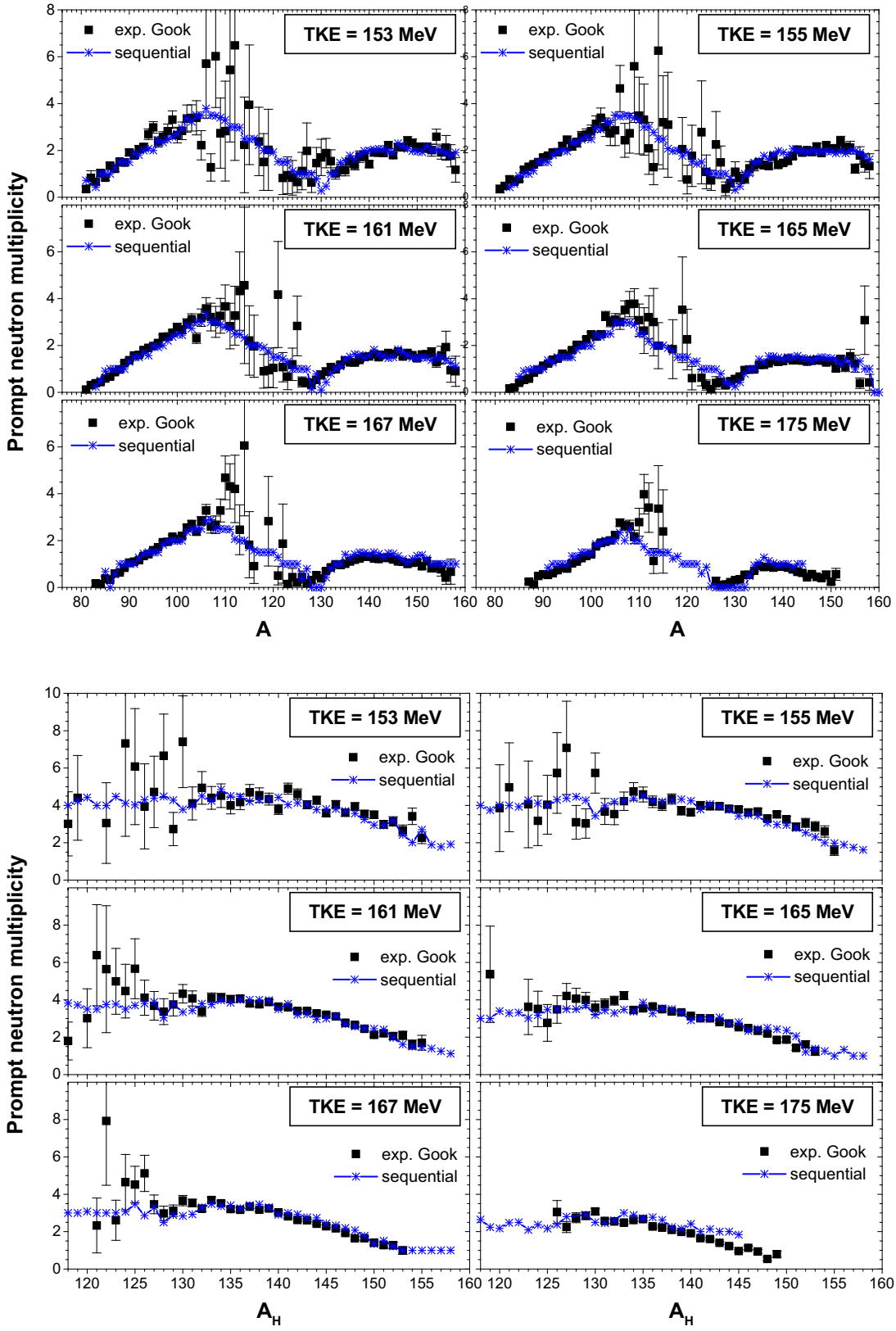

Fig. 4. Comparison of the $\nu(A, \mathrm{TKE})$ matrix of sequential emission (blue stars) for $^{235}\mathrm{U}(\mathrm{n_{th}}, \mathrm{f})$ with the data of Göök *et al.* (black squares) in the representation of the prompt neutron multiplicity as a function of A (upper part) and as the prompt neutron multiplicity of fragment pair as a function of A_{H} (lower part) at the TKE values indicated in each frame. The lines connecting the points plotted with stars are only to guide the eye.

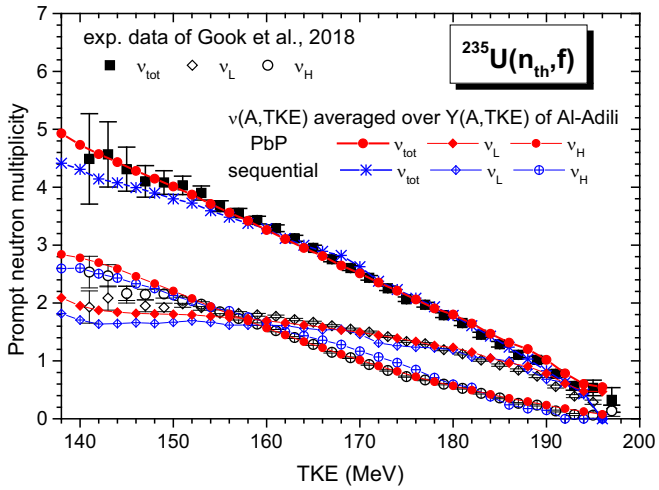

Fig. 5. The results of $\langle\nu_{tot}\rangle$(TKE), $\langle\nu_L\rangle$(TKE) and $\langle\nu_H\rangle$(TKE) of PbP (red symbols) and of sequential emission treatment (blue symbols) in comparison with the experimental data of Göök *et al.* (black symbols).

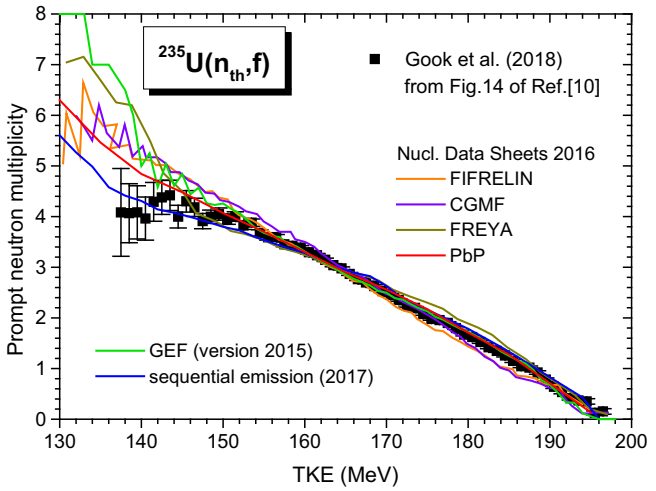

Fig. 6. The predicted $\langle\nu\rangle$(TKE) results (lines) of FIFRELIN (orange), CGMF (violet), FREYA (dark yellow), PbP (red), GEF (green) and of the sequential emission treatment (blue) in comparison with the subsequent data of Göök *et al.* (black squares) reported in fig. 14 of ref. [10].

3.2 Secondary validation of models together with an experimental Y(A,TKE) distribution

Single distributions of different prompt emission quantities (*e.g.* $\nu(A)$, ν(TKE), $E_\gamma(A)$, $\langle\varepsilon\rangle(A)$ etc.) and total average quantities (*e.g.* prompt neutron spectra in the center-of-mass and laboratory frames, total average prompt neutron multiplicity etc.) can be obtained by averaging the multi-parametric matrices of these quantities over a multiple fission fragment distribution.

PbP and sequential emission results of $\nu(A)$ and $\langle\varepsilon\rangle(A)$ for ^{235}U(n$_{th}$, f) were already reported in refs. [5, 7]. They were obtained by averaging the corresponding multi-parametric matrices over TKE using the experimental $Y(A, \mathrm{TKE})$ data of Al-Adili *et al.* [15]. A larger step size of the TKE range, *i.e.* of 5 MeV, was used at that time. These results were compared in refs. [5,7] with the preliminary data of Göök *et al.* reported in 2017 during the workshop Theory-4 [16].

Because the single distributions as a function of A, obtained in this work (using a TKE step size of 2 MeV) are only slightly improved compared to the ones of refs. [5, 7] and the differences between the data of Göök *et al.* for $\nu(A)$ and $\langle\varepsilon\rangle(A)$ reported in ref. [10] and the preliminary ones of ref. [16] are less visible in graphical representations, both model results for average prompt emission quantities as a function of A are given in the appendix.

Data of Göök *et al.* concerning the average prompt neutron multiplicity as a function of TKE are now available not only for all fragments but also separately for the light and heavy fragment groups. They are plotted in fig. 5 with full black squares for $\langle\nu_{tot}\rangle$(TKE), open diamonds for $\langle\nu_L\rangle$(TKE) and open circles for $\langle\nu_H\rangle$(TKE). As it can be seen all these data are very well described by the results of both modelings (red symbols for PbP and blue symbols for sequential emission).

The remarkable description of the experimental data of $\langle\nu_{tot}\rangle$(TKE) as well as of the components $\langle\nu_L\rangle$(TKE) and $\langle\nu_H\rangle$(TKE) by the PbP result (red symbols) deserves to be mentioned.

The sequential emission result (blue symbols) describes well the experimental $\langle\nu_{tot}\rangle$(TKE), $\langle\nu_L\rangle$(TKE) and $\langle\nu_H\rangle$(TKE) data, too. At low TKE values, below 150 MeV, the sequential emission results are a little bit lower than the PbP results. This is not surprising because at low TKE values the prompt neutron multiplicities of fragment pairs (see the red lines in figs. 1 and 2) provided by the sequential emission calculation are a little bit lower than the PbP results for a great part of fragmentations. This fact confirms again that the use of a residual temperature distribution in the PbP treatment can better cover the entire process of sequential emission corresponding to each initial fragment at each TKE value compared to a deterministic treatment of the successive neutron emission from a limited number of initial fragments taken at each A and TKE. The use in the sequential emission treatment [7] of non-energy dependent level density parameters of initial and residual fragments has an influence, too.

It is interesting to mention that the $\langle\nu\rangle$(TKE) data of Göök *et al.* which are reported in fig. 14 of ref. [10] confirm the predictions of six model codes, plotted with lines in fig. 6. *I.e.*, the $\langle\nu\rangle$(TKE) results of four computer codes: FIFRELIN (orange), CGMF (violet), FREYA (dark yellow) and PbP (red) reported in 2016 ref. [1], the result of GEF (version 2015) [17] (green) and also the preliminary result of sequential emission (blue) reported during the workshop Theory-4 (2017) [18].

It can be also observed that at TKE values above of about 145 MeV the best description of the experimental $\langle\nu\rangle$(TKE) data is accomplished by the results of PbP (red) and GEF (green). At low TKE values, below 145 MeV, the data from ref. [10] are better described by the sequential emission result (blue).

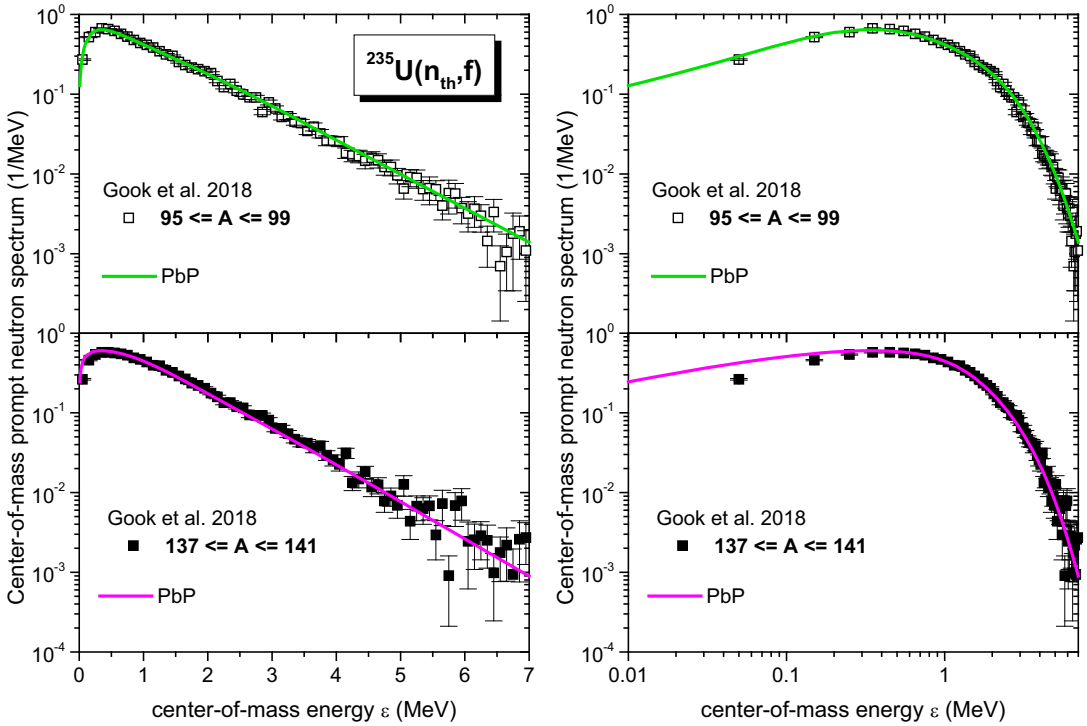

Fig. 7. The experimental prompt neutron spectrum in the center-of-mass frame for selected fragment mass ranges around the most probable fragmentation from ref. [10] (light fragments in the upper part and heavy fragments in the lower part) and the PbP results representing the spectrum obtained by averaging the multi-parametric matrix $\Phi(\varepsilon, A, Z, \mathrm{TKE})$ separately over the light and heavy fragment groups. The high energy part of the spectrum is focused in the left part of the figure and the low energy part of the spectrum in the right part.

Note that the $\langle\nu\rangle$(TKE) data reported in fig. 14 of ref. [10], which are plotted in fig. 6, are given at the middle of TKE bins (*i.e.* TKE values going from 137.5 MeV up to 196.5 MeV with a step size of 1 MeV), while the $\langle\nu\rangle$(TKE) data plotted with full black squares in fig. 5 are obtained from the experimental $\nu(A, \mathrm{TKE})$ data of figs. 1–4, which are given at odd TKE values (starting from 141 MeV). *I.e.*, the experimental data of $\langle\nu\rangle$(TKE), $\langle\nu_{\mathrm{L}}\rangle$(TKE) and $\langle\nu_{\mathrm{H}}\rangle$(TKE) plotted in fig. 5 are at odd TKE values going from 141 to 197 MeV.

Experimental data of the prompt neutron spectrum in the center-of-mass frame $\Phi(\varepsilon)$ are very scarce, almost inexistent. Fortunately the recent experimental data for this quantity reported in ref. [10] offer the possibility of a valuable comparison with the model results. Such comparison is exemplified in the next figures as follows.

Figure 7 shows the experimental center-of-mass energy spectrum of prompt neutrons reported by Göök *et al.* [10] for selected fragment mass ranges around the most probable fragmentation mentioned in the legend of each frame (light fragments in the upper part and heavy fragments in the lower part). These data are very well described over the entire energy range by the model results obtained from the matrix $\Phi(\varepsilon, A, \mathrm{TKE})$ which was averaged separately over the distributions [15] of the light and heavy fragment groups. For a better visualization the high and low energy parts of the spectra are focused in separate frames.

The center-of-mass energy spectrum data corresponding to all fragments [10] plotted in fig. 8 are also well

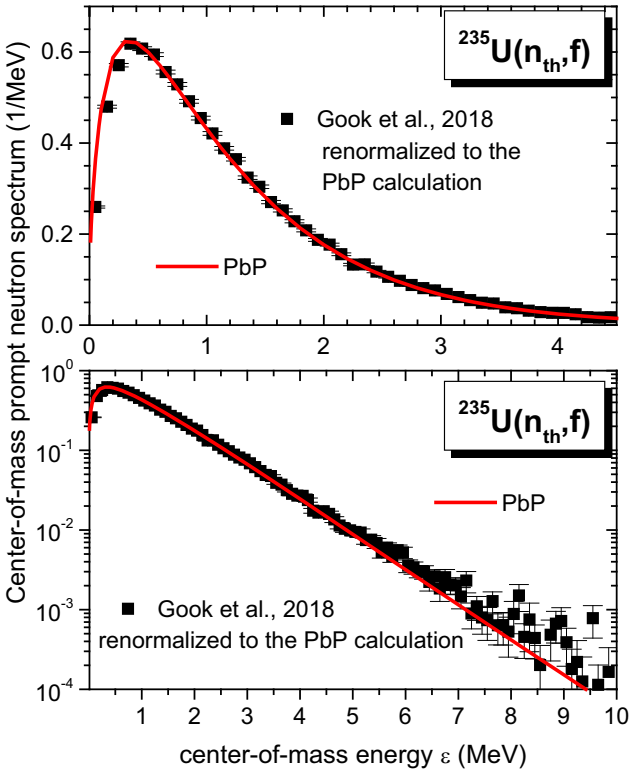

Fig. 8. Experimental data of the prompt neutron spectrum in the center-of-mass frame of Göök *et al.* (black squares) and the $\Phi(\varepsilon)$ result (red line) from the PbP calculation. The experimental data are re-normalized to the calculated spectrum.

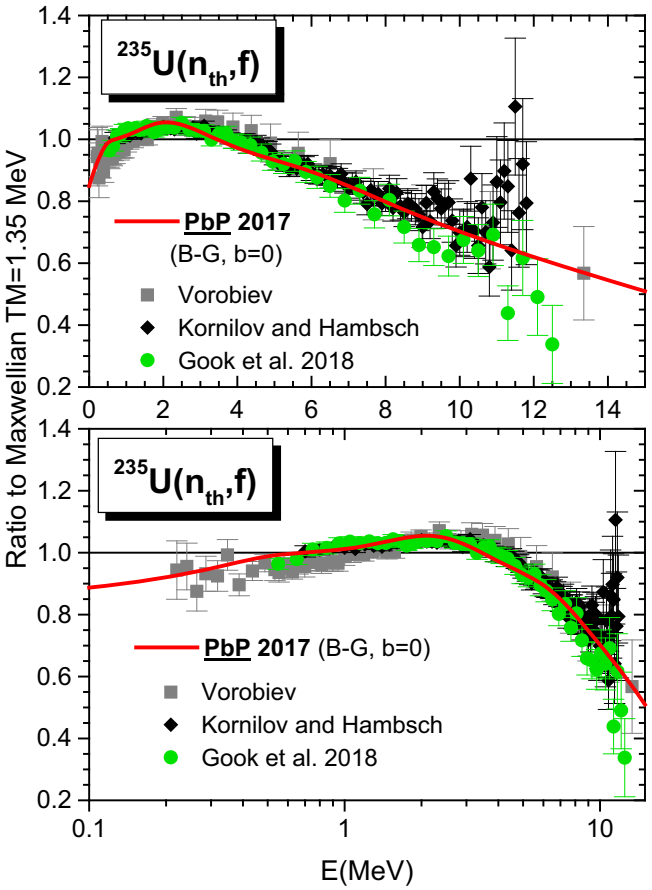

Fig. 9. Comparison of the PFNS data of Göök *et al.* (green circles) with the previous PbP result [5] (red line) and the previous data of Kornilov and Hambsch measured at thermal En (black diamonds) and the data of Vorobiev *et al.* (gray squares) in the usual representation as a ratio to a Maxwellian spectrum (with $TM = 1.35\,\mathrm{MeV}$). All experimental data sets were re-normalized to the PbP calculation.

described by the model result over the entire prompt neutron energy range, only at energies above 7 MeV a slight underestimation of a great part of the scattered experimental data with large error bars is observed.

Consequently the recent experimental data of $\Phi_{\mathrm{L,H}}(\varepsilon)$ and $\Phi(\varepsilon)$ reported by Göök *et al.* [10] confirm the results of the model calculation previously performed [5].

The experimental prompt fission neutron spectrum in the laboratory frame (PFNS) measured by Göök *et al.* [10] is plotted in fig. 9 with green circles, in the usual representation as a ratio to a Maxwellian spectrum. It is compared with the previous experimental data on thermal and cold neutron fission of ^{235}U from ref. [19] (black diamonds) and ref. [20] (gray squares). These data sets are re-normalized to the PFNS result at thermal En of ref. [5] (plotted with a red line). The spectral shape of Göök *et al.* data agrees within the uncertainty with the previous experimental data on thermal and cold neutron induced fission. A slight softening of the PFNS of Göök compared to the previous experimental data and the model result is observed at high energies, however within the estimated experimental uncertainty.

The very good description of all experimental single distributions of different prompt emission quantities as well as of prompt neutron spectra in the center-of-mass and laboratory frames by the model results (obtained by averaging the corresponding multi-parametric matrices as primary model results over an experimental fragment distribution) validates the PbP and sequential emission models together with the $Y(A, \mathrm{TKE})$ distribution of Al-Adili *et al.* [15].

4 Conclusions

The recent experimental investigation of prompt fission neutrons of ^{235}U (performed at the GELINA facility of JRC-Geel) is very important and welcome offering the possibility to compare the new experimental data for many quantities with the results of prompt emission models.

The very good description of the recent $\nu(A, \mathrm{TKE})$ data of Göök *et al.* [10] by the prompt neutron multi-parametric matrices $\nu(A, \mathrm{TKE})$, which are the primary results of the PbP and sequential emission calculations previously performed [5,7], constitutes a valuable validation of the PbP and sequential emission modelings themselves (because the fragment distributions $Y(A, \mathrm{TKE})$ are not involved).

The data of Göök *et al.* concerning the single distributions of different prompt emission quantities as well as the total average prompt neutron spectrum in the center-of-mass frame $\Phi(\varepsilon)$ and laboratory frame $N(E)$ are also well described by both model results which were obtained by averaging the corresponding multi-parametric matrices over an experimental $Y(A, \mathrm{TKE})$ distribution measured at JRC-Geel [15]. This fact can be considered as a secondary validation of both deterministic models of prompt emission together with the fragment distribution $Y(A, \mathrm{TKE})$ mentioned above.

Taking into account the scarcity of experimental data for the prompt neutron spectrum in the center-of-mass frame, the very good description of the data of Göök *et al.* [10] concerning the center-of-mass energy spectra for selected fragment mass ranges around the most probable fragmentation and for all fragments by the model results deserves a special mentioning.

This work was done in the frame of the Romanian Project PN-III-P4-PCE-2016-0014 (Contract no.7/2017). Thanks to Franz-Josef Hambsch and Alf Göök for the interesting discussions during this work and for providing experimental data.

Data Availability Statement This manuscript has no associated data or the data will not be deposited. [Author's comment: All data generated during this study are contained in this published article.]

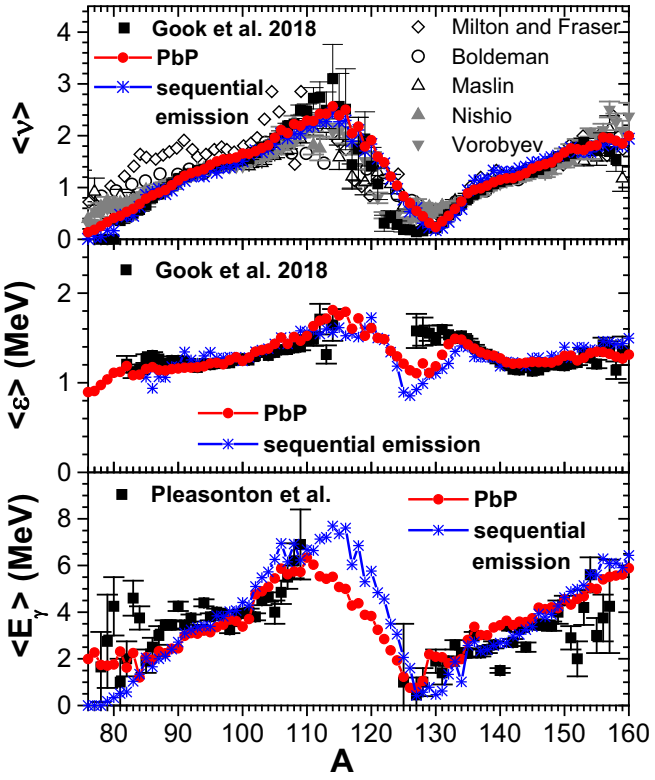

Fig. 10. PbP and sequential emission results of $\nu(A)$ (upper part), $\langle\varepsilon\rangle(A)$ (middle) and $\langle E_\gamma\rangle(A)$ (lower part) in comparison with the experimental data. The lines connecting the points are only to guide the eye.

Appendix A.

The PbP and sequential emission results of $\nu(A)$, $\langle\varepsilon\rangle(A)$ and $\langle E_\gamma\rangle(A)$, obtained by averaging the corresponding matrices over TKE (with a step size of 2 MeV) using the experimental $Y(A, \mathrm{TKE})$ data of Al-Adili *et al.* [15], are plotted in fig. 10 with red circles and blue stars, respectively.

As can be seen in the upper part both $\nu(A)$ results describe well the recent data of ref. [10] (black squares) and the previous data from the EXFOR library [21] (different open black and full gray symbols). They exhibit a minimum at A_H around 130 (due to the magic and/or double magic heavy fragments with $N = 82$ and/or $Z = 50$ which emit prompt neutrons with a great difficulty) while the $\nu(A)$ data of Göök exhibit a smoother minimum which is shifted to A_H of about 127–128 compared to other experimental data.

Both $\langle\varepsilon\rangle(A)$ results (middle part of fig. 10) are in good agreement with the experimental data of Göök *et al.* [10]. The model results are close to each other except for A between of about 120–130 where the sequential emission result is significantly lower (due to the limited number of fragments at each A which are able to emit prompt neutrons and the approximations used to solve the successive transcendent equations of residual temperature).

Nevertheless some differences between the experimental $\langle\varepsilon\rangle(A)$ data and the model results are observed. They are significant at A around 125–130 and are visible at $A < 90$.

A possible cause of these differences is related to how the first order momentum of an energy spectrum is determined, as follows.

The model result of $\langle\varepsilon\rangle(A)$ is obtained from the multiparametric matrix $\langle\varepsilon\rangle(A, Z, \mathrm{TKE})$ which is the first order momentum of the prompt neutron spectrum in the center-of-mass frame $\Phi(\varepsilon, A, Z, \mathrm{TKE})$ (corresponding to each fragment at each TKE value).

The experimental data of prompt neutron spectra in the center-of-mass frame (corresponding to all fragments and to selected fragment mass ranges around the most probable fragmentation, $95 \leq A \leq 99$ and $137 \leq A \leq 141$) are very well described by the model results, see figs. 7 and 8.

To obtain $\langle\varepsilon\rangle$ as the first order momentum of an experimental center-of-mass energy spectrum, the integration must be done over the entire energy range. For this reason the experimental $\Phi(\varepsilon)$ data (which are not measured over the entire ε range) must be fitted with a theoretical spectrum. In the majority of cases the experimentalists use Maxwellian spectra. The experimental $\Phi(\varepsilon)$ data of Göök *et al.* are fitted with Maxwellian spectra, too (see *e.g.*, fig. 9 and 10 of ref. [10]). The obvious differences in shape between the Maxwellian spectrum (fitting satisfactory the experimental data measured in a limited energy range) and the spectrum provided by a model (which also describes well the same experimental data) are reflected in differences between their first order momenta.

Even if the aim of this work was the comparison with recent experimental data, the $\langle E_\gamma\rangle(A)$ results (lower part of fig. 10) are compared with old experimental data [22] because —to our knowledge— they are the unique data available for this quantity. Albeit visible differences exist between the $\langle E_\gamma\rangle(A)$ results, both succeed to describe the data. The differences are significant near symmetry where the data are missing. The higher $\langle E_\gamma\rangle(A)$ result of sequential emission near symmetry is due to a lower energy carried away by each neutron successively emitted compared to the average energy carried away per neutron in the case of PbP which includes a global treatment of sequential emission by a residual temperature distribution.

References

1. R. Capote, Y.J. Chen, F.-J. Hambsch, N.V. Kornilov, J.P. Lestone, O. Litaize, B. Morillon, D. Neudecker, S. Oberstedt, T. Ohsawa, N. Otuka, V.G. Pronyaev, A. Saxena, O. Serot, O.A. Shcherbakov, N.C. Shu, D.L. Smith, P. Talou, A. Trkov, A.C. Tudora, R. Vogt, S. Vorobyev, Nucl. Data Sheets **131**, 1 (2016).
2. O. Litaize, O. Serot, L. Thulliez, A. Chebboubi, EPJ Web of Conferences **146**, 09006 (2017).
3. O. Litaize, L. Thulliez, O. Serot, A. Chebboubi, P. Tamagno, EPJ Web of Conferences **169**, 00012 (2018).
4. P. Talou, R. Vogt, J. Randrup, M.E. Rising, S.A. Pozzi, J. Verbeke, M.T. Andrews, S.D. Clarke, P. Jaffke, M. Jandel, T. Kawano, M.J. Marcath, K. Meierbachtol, L. Nakae, G.

Rusev, A. Sood, I. Stetcu, C. Walker, Eur. Phys. J. A **54**, 9 (2018).
5. A. Tudora, F.-J. Hambsch, Eur. Phys. J. A **53**, 159 (2017).
6. A. Göök, F.-J. Hambsch, M. Vidali, Phys. Rev. C **90**, 064611 (2014).
7. A. Tudora, F.-J. Hambsch, V. Tobosaru, Eur. Phys. J. A **54**, 87 (2018).
8. EXFOR Experimental Nuclear Data Library (available online at `https://www-nds.iaea.org`) nucleus U-233, reaction (n,f), quantity MFQ, entry 22660008/1998Ni16 (Nishio).
9. A. Tudora, A. Matei, Rom. J. Phys. **64**, 301 (2019).
10. A. Göök, F.-J. Hambsch, S. Oberstedt, M. Vidali, Phys. Rev. C **98**, 044615 (2018).
11. A.C. Wahl, At. Data Nucl. Data Tables **39**, 1 (1988).
12. A. Tudora, F.-J. Hambsch, I. Visan, G. Giubega, Nucl. Phys. A **940**, 242 (2015).
13. R. Capote, M. Herman, P. Oblozinsky, P.G. Young, S. Goriely, T. Belgya, A.V. Ignatiuk, A.J. Koning, S. Hilare, V.A. Plujko, M. Avrigeanu, O. Bersillon, M.B. Chadwick, T. Fukahory, Zhigang Ge, Yinlu Han, S. Kailas, J. Kopecky, V.M. Maslov, G. Reffo, M. Sin, E.Sh. Soukhovitskii, P. Talou, Nucl. Data Sheets **110**, 3107 (2009) and IAEA-RIPL3 electronic library, available online at `https://www-nds.iaea.org`, segment IV, *Optical model parameters*, (Becchetti-Greenlees and Koning-Delaroche).
14. F.-J. Hambsch, A. Göök, private communication (2018).
15. A. Al-Adili, F.-J. Hambsch, S. Pomp, S. Oberstedt, Phys. Rev. C **86**, 054601 (2012).
16. A. Göök, F.-J. Hambsch, S. Oberstedt, EPJ Web of Conferences **169**, 00004 (2018).
17. K.-H. Schmidt, B. Jurado, C. Amouroux, C. Schmitt, Nucl. Data Sheets **131**, 107 (2016).
18. A. Tudora, F.-J. Hambsch, EPJ Web of Conferences **169**, 00025 (2018).
19. N.V. Kornilov, F.-J. Hambsch, I. Fabry, S. Oberstedt, T. Belgya, Z. Kis, L. Szentmiklosi, S. Simakov, Nucl. Sci. Eng. **165**, 117 (2010).
20. A.S. Vorobyev, A. Shcherbakov, IAEA report INDC(CCP)-0455, English translation of selected papers published in Voprosy Atomhnoj Nauki I Tekniki, Series Yadernye Konstanty (Nuclear Constants), Issue No. 1-2 (2011-2012).
21. EXFOR Experimental Nuclear Data Library (available online at `https://www-nds.iaea.org`) nucleus U-235, reaction (n,f), quantity MFQ: entries 14369003 (Milton and Fraser), 30909004 (Boldeman), 21095002-004 (Maslin), 22464004 (Nishio), 41516012 (Vorobyev).
22. F. Pleasonton, R.L. Ferguson, H.W. Schmitt, Phys. Rev. C **6**, 1023 (1972).